X-ray Absorption Spectroscopy of the Zinc-Binding Sites in the Class B2 Metallo-β-lactamase ImiS from *Aeromonas veronii bv. sobria*[†]

Alison L. Costello,[‡] Narayan P. Sharma,[§] Ke-Wu Yang,[§] Michael W. Crowder,[§] and David L. Tierney*[,‡]

Department of Chemistry, University of New Mexico, Albuquerque, New Mexico 87131-0001, and Department of Chemistry and Biochemistry, Miami University, Oxford, Ohio 45056

Received July 31, 2006; Revised Manuscript Received September 15, 2006

ABSTRACT: X-ray absorption spectroscopy was used to investigate the metal-binding sites of ImiS from *Aeromonas veronii bv. sobria* in catalytically active (1-Zn), product-inhibited (1-Zn plus imipenem), and inactive (2-Zn) forms. The first equivalent of zinc(II) was found to bind to the consensus Zn_2 site. The reaction of 1-Zn ImiS with imipenem leads to a product-bound species, coordinated to Zn via a carboxylate group. The inhibitory binding site of ImiS was examined by a comparison of wild-type ImiS with 1 and 2 equiv of bound zinc. 2-Zn ImiS extended X-ray absorption fine structure data support a binding site that is distant from the active site and contains both one sulfur donor and one histidine ligand. On the basis of the amino acid sequence of ImiS and the crystal structure of CphA [Garau et al. (2005) *J. Mol. Biol. 345*, 785−795], we propose that the inhibitory binding site is formed by M146, found on the B2-distinct α3 helix, and H118, a canonical Zn_1 ligand, proposed to help activate the nucleophilic water. The mutation of M146 to isoleucine abolishes metal inhibition. This is the first characterization of ImiS with the native metal Zn and establishes, for the first time, the location of the inhibitory metal site.

The β-lactamases, by conferring resistance to the most heavily prescribed antibiotics, pose an ever-increasing threat to human health, as more and more pathogenic organisms obtain them. The majority of β-lactamases [ca. 80−90%, classes A, C, and D (*1*)] utilize a serine side chain to perform a nucleophilic attack on the β-lactam ring, converting it to an inactive, ring-opened form. Metallo-β-lactamases (MβLs,[1] class B) require one to two Zn ions for full activity (*2*−*5*). Unlike the serine-active lactamases, MβLs have no known clinically effective inhibitors.

In general, the MβLs exhibit broad substrate profiles, although all show some preference for different classes of substrates. The MβLs are divided into three subclasses based on sequence homology and substrate affinity (*6*). Group B1 enzymes share >23% sequence identity, reach full activity with 2 equiv of zinc, and preferentially hydrolyze penicillins and cephalosporins [representative examples include BcII from *Bacillus cereus* (*7*, *8*) and CcrA from *Bacteroides fragilis* (*9*, *10*)]. Group B3 lactamases display similar characteristics, including a requirement for two Zn ions, while conserving only 9 amino acids and preferring cephalosporins as substrates [representative examples include L1 from *Stenotrophomonas maltophilia* (*11*) and GOB from *Elizbethkingia meningiosepticum* (*12*)]. The most unusual members of the metallo-β-lactamase family belong to Group B2, found chiefly in *Aeromonas* species (*13*, *14*). The B2 enzymes share 11% sequence identity with Group B1, but only 1 equiv of zinc is required for full activity. The B2 enzymes also show very narrow substrate profiles, almost exclusively hydrolyzing carbapenems.

Considerable information exists regarding the B1 and B3 enzymes, including X-ray diffraction (*15*−*29*), spectroscopic (*9*, *30*−*42*), mechanistic (*43*−*59*), and computational studies (*60*−*72*). The B2 enzymes are less well-characterized, with comparably fewer physicochemical studies available (*73*−*81*). Recently, the first crystal structure of a B2 enzyme was reported (*82*). The structure of CphA from *Aeromonas hydrophila* unexpectedly showed that the first, hydrolytic equivalent of zinc binds to the consensus Zn_2 site, in contrast to the B1 and B3 subclasses in which the primary, hydrolytic zinc binds to the Zn_1 site (*41*, *42*).

The X-ray structure (*82*) and a previous extended X-ray absorption fine structure (EXAFS) study (*77*) of CphA are currently the only direct examinations of a B2 β-lactamase in its catalytically active, monozinc form. A similar binding site, on the basis of cobalt substitution, has been predicted for ImiS from *Aeromonas veronii*, which shares 98% amino acid sequence identity with CphA (*79*). An alternative model, suggesting that the catalytic metal ion is either labile (distributed between the two sides of the active site) or resides in a site made up of ligands from both sites has been put forth for AE036 from *A. hydrophila* (*77*). Kinetic data for both CphA and ImiS show that a second equivalent of zinc acts as a noncompetitive inhibitor of enzymatic activity (*76*, *78*). At present, the only structural information regarding this second, inhibitory binding site is for the cobalt analogue of ImiS (*79*), where electron paramagnetic resonance (EPR)

[†] This work was supported by the National Institutes of Health (NCRR P20RR-16480 to D.L.T. and GM40052 to M.W.C.). The National Synchrotron Light Source is supported by the U.S. Department of Energy.

* To whom correspondence should be addressed. Telephone: (505) 277-2505. Fax: (505) 277-2609. E-mail: dtierney@unm.edu.

[‡] University of New Mexico.

[§] Miami University.

[1] Abbreviations: EXAFS, extended X-ray absorption fine structure; MβL, metallo-β-lactamase; XAS, X-ray absorption spectroscopy.

10.1021/bi061547e CCC: $33.50
Published on Web 10/20/2006

and nuclear magnetic resonance (NMR) data were interpreted as indicative of a remote (>7 Å) binding site for the inhibitory metal ion. To examine the generality of the metal site reported for CphA within Group B2 β-lactamases, detailed structural information is needed on the metal-binding sites of more B2 enzymes. In this paper, we present EXAFS characterization of catalytically active, monozinc ImiS and its product complex with hydrolyzed imipenem. The dizinc forms of both the wild-type and a mutant enzyme are also examined, defining for the first time the location of the inhibitory binding site.

EXPERIMENTAL PROCEDURES

One- and two-Zn forms of wild-type ImiS were prepared and characterized kinetically according to published procedures (*78*). Using the PAGE-purified oligonucleotide primers and the overexpression plasmid for ImiS (pET26b-imiS) as a template, the ImiS mutant was generated using the Quikchange site-directed mutagenesis kit, according to the instructions of the manufacturer. The primers used for the mutagenesis studies were M146IFor, GCCCAGTCGCTCT-TGATCAGATCCCGGGT; and M146IRev, ACCCGG-GATCTGATCAA GAGCGACTGGGC. DNA sequencing of the mutated *imiS* gene using T7for (TAATACgACTCAC-TATAgg) and T7rev (CgATCAATAACGAgTCgCC) as primers was used to confirm the presence of the intended mutation and the absence of other, unintended mutations. These DNA sequences were analyzed on a Perkin-Elmer ABI 3100 genetic analyzer. To test for the overexpression of mutants, the mutant plasmids were transformed into *Escherichia coli* BL21(DE3) cells and small-scale cell cultures were grown. Metal content and steady-state kinetic constants were determined as previously reported (*78*).

Samples for EXAFS (1−2 mM) were prepared with 20% (v/v) glycerol as a cryoprotectant, preloaded in Lucite cuvettes with 6 μm polypropylene windows, and frozen rapidly in liquid nitrogen. X-ray absorption spectroscopy (XAS) data were measured at the National Synchrotron Light Source (NSLS), beamline X9B, using a Si (111) double-crystal monochromator and a Ni-focusing mirror for harmonic rejection. Data collection and reduction were performed according to published procedures (*42*, *83*). X-ray absorption spectra of each ImiS variant were measured on two individually prepared samples (8 scans per sample). The two datasets for each variant were compared. In each case, the two datasets gave comparable results; they were averaged, and it is the averages that are presented here.

The resulting $\chi(k)$ EXAFS data were fit (∼9 degrees of freedom for single-scattering and 30 degrees of freedom for multiple-scattering fits) using the nonlinear least-squares algorithm contained in IFEFFIT, interfaced with SixPack (Sixpack is available free of charge from http://www-ssrl.slac.stanford.edu/∼swebb/index.htm). The scale factor, S_c, and ΔE_0 were calibrated by fitting experimental data for compounds of known structure, holding all other parameters fixed. Models used for calibration were *tetrakis*-1-methylimidazole zinc(II) perchlorate, $Zn(MeIm)_4$, for Zn−N interactions and tetramesitylthiolate zinc(II), $Zn(Smes)_4$, for Zn−S scattering. The optimum value of ΔE_0 was −21 eV for both; scale factors were Zn−N = 0.78 and Zn−S = 0.91. Fits were carried out for all reasonable coordination numbers, holding S_c and ΔE_0 constant, while varying R_{as} and σ_{as}^2. Fits to unfiltered data gave similar results.

Multiple-scattering contributions from histidine ligands were approximated by fitting FEFF calculated paths, derived from the crystallographic coordinates of $Zn(MeIm)_4$, to the experimental EXAFS of $Zn(MeIm)_4$ (*84*). The best fits resulted in four prominent multiple-scattering features (representing 140 total scattering paths); paths of similar overall length were combined to match these four features (*42*). The combined paths were used to fit protein data, fixing the number of imidazole ligands per metal ion at integral or half-integral values, while varying R_{as} and σ_{as}^2. The uncertainty in the number of histidines, determined in this way, is estimated to be ±0.5.

RESULTS

Previous steady-state kinetic studies have shown that the recombinant ImiS utilized for the present studies displays catalytic constants similar to those found for native ImiS (*78*) and CphA (*73*) and that ImiS shows a preference for carbapenem substrates, typical of class B2 MβLs. The first equivalent of Zn binds to ImiS with a K_d < 2 nM (*78*). The addition of a second equivalent of zinc was found to noncompetitively inhibit the enzyme, with a K_i of 15 ± 4 nM (*78*). These results confirm that the recombinant ImiS used for the present EXAFS studies binds the first equivalent of Zn^{II} in the active site and the second equivalent at the inhibitory site.

Resting, Monozinc Enzyme. The EXAFS data for the hydrolytically active, monozinc form of ImiS (1-Zn ImiS, Figure 1) show an asymmetric first shell, centered at $R + \alpha \approx 1.5$ Å, with a significant shoulder to higher *R*. Single-scattering fits, summarized in Table 1, using only low-Z scatterers refine to an average of 4 N/O scatterers (fit 1-1) at a distance of 2.08 Å; distinct oxygen and nitrogen shells could not be resolved. Inclusion of a sulfur donor improves the fit residual 20-fold (fit 1-2), clearly demonstrating that the first, catalytically relevant Zn ion coordinates the cysteinate of the Zn_2 site. The multiple-scattering fit in Figure 1 is the sum of single-scattering contributions (3N/O, 1S) and one rigid imidazole ligand (fit 1-3). While Asp120 is expected to be a ligand to the Zn ion, inclusion of a Zn−C (carboxylate) interaction did not significantly improve the fit. This is not uncommon, given the complexity of the multiple-scattering fit (*42*). Attempts to include a Zn−Zn interaction, consistent with the formation of a dinuclear cluster (*42*, *83*), resulted in an *increase* in the fit residual, suggesting that distributed or scrambled binding of Zn does not occur.

Enzyme−Product Complex. The B2 lactamases are known to display product inhibition (*78*, *82*). It was therefore possible to prepare a product complex of ImiS with the hydrolyzed product of its reaction with imipenem. In the crystal structure report for CphA (*82*), it was suggested that the Zn ion was five-coordinate, with a ligand set comprised of the three constitutive protein ligands and both the N4 nitrogen atom, formerly part of the β-lactam ring, and an oxygen atom from the auxiliary carboxylate. In the reaction scheme that was proposed, the final complex was four-coordinate, with the nitrogen atom having been protonated and released. A minimal change is seen in the X-ray

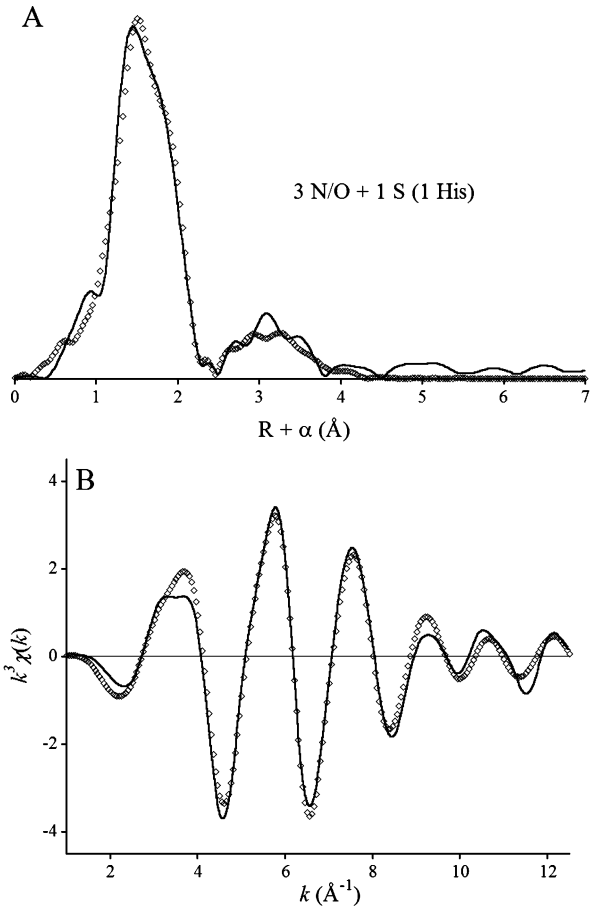

FIGURE 1: Fourier transforms (A) of experimental k^3-weighted EXAFS data (B) for 1-Zn ImiS (—) and best fit (◇).

absorption near edge structure (XANES) between 1-Zn ImiS and the 1-Zn ImiS product complex (Figure S1 in the Supporting Information), indicating that the average Zn environment in the two forms is similar. EXAFS data for the enzyme−product complex of 1-Zn ImiS with hydrolyzed imipenem (Figure 2) indicate that the primary coordination sphere is generally the same as it is in the resting enzyme. Single-scattering fits to the first shell, using only low-Z scatterers, refine to an average of four nitrogen/oxygen donors at 2.07 Å (fit 2-1), nearly identical to 1-Zn ImiS (fit 1-1). The addition of one sulfur ligand at 2.30 Å leads to a 93% improvement in the first shell fit (compare fit 2-2 to 2-1). A small rearrangement in the outer shell scattering is apparent in both the *k*- and *R*-space data, but there is no increase in intensity. The best fit, presented in Figure 2 (fit 2-3), consists of a first shell of three N/O and one S donor, with multiple-scattering contributions from one coordinated histidine. Inclusion of carboxylate carbon scattering or outer shell scattering from another ring structure (as would be anticipated for the coordination of the product through the N4 nitrogen) did not improve the fit. Thus, the ImiS plus imipenem product complex is more consistent with the end-stage complex proposed but not observed for CphA (*82*).

Zinc-Inhibited Enzyme. The addition of a second equivalent of Zn^{II} to 1-Zn ImiS affords the Zn-inhibited form of the enzyme. The two give nearly identical XANES spectra, aside from a small shift (~0.3 eV) to lower energy and slightly more intense white-line absorption with the additional Zn (Figure S1 in the Supporting Information). When the EXAFS of 1-Zn and 2-Zn ImiS was compared (Figure 3), the center of gravity of the FTs main peak shifts to higher *R*, with little change in the outer shell scattering. The best first shell fit, utilizing all low-Z scatterers, consists of an average of 4 N/O scatterers per zinc ion at a distance of 2.10 Å (fit 3-1); separate nitrogen and oxygen shells could not be resolved. Inclusion of 0.5 sulfur ligands, maintaining the cysteinate ligand to the catalytic metal with no heavy scatterers coordinated to the inhibitory metal, results in a significant improvement in the fit residual (84%) but gives an unreasonably low Debye−Waller factor for the sulfur (3×10^{-8} Å^2). However, increasing the sulfur coordination number to 1 restores the Debye−Waller factor while improving the fit residual by 86% (compare fit 3-1 to 3-2 in Table 1). Increasing the sulfur coordination number in half-integer increments beyond a value of 1 did not further improve the fit residual and resulted in unreasonable R_{as} and σ_{as}^2 (not shown), suggesting that the inhibitory metal also coordinates one sulfur atom. The outer shell scattering for 2-Zn ImiS is nearly indistinguishable from that of 1-Zn ImiS and is best modeled with an average of 1 histidine ligand per zinc ion (Figure 4). Inclusion of a Zn−Zn interaction or a $Zn-C_{CO_2}$ resulted in unreasonable distances and failed to improve fit residuals.

The EXAFS data for 2-Zn^{II}−ImiS indicate that the coordination sphere of the second, inhibitory zinc ion includes one sulfur ligand and one histidine residue. Given the surprisingly large amplitude of the sulfur scattering observed for the Zn-inhibited enzyme, we sought to identify the source through mutation. Only one cysteine residue is present in the amino acid sequence of ImiS, and that cysteine coordinates the catalytic metal ion. We therefore turned our attention to the four methionines present: M43, M72, M146, and M252 (*85*). The slight increase in Zn−S distance from 1-Zn (2.28 Å) to 2-Zn ImiS (2.33 Å) is consistent with an average of an equal number of thiolate and thioether donors in 2-Zn ImiS. Because ImiS and CphA share >98% sequence identity, the crystal structures of CphA and CphA plus biapenem (*82*) were used as a guide in locating the inhibitory metal site.

As detailed in the Discussion below, M146, which is contained in a loop that encloses the active site when the substrate binds, appeared the most likely candidate. We therefore prepared the isoleucine mutant of M146. The M146I mutant bound the hydrolytic metal ion with a K_d < 2 nM and exhibited steady-state kinetic constants of $k_{cat} = 197 \pm 11$ s^{-1} and $K_m = 103 \pm 12$ μM at pH 7.0 when using imipenem as the substrate, only slightly less effective (~30%) than the wild-type enzyme (*78*). Metal analyses showed that the mutant is isolated with 1 equiv of Zn^{II} bound. Unlike wild-type enzyme, which was inhibited by nearly 70% when incubated with 20 nM Zn^{II}, the M146I mutant showed no measurable decrease in activity with 20 nM Zn^{II}.

XANES spectra for the wild-type and mutant enzymes show a dramatic increase in white line absorption upon mutation of M146 to isoleucine (Figure S1 in the Supporting Information), suggesting the second equivalent of Zn coordinates multiple water ligands and may be hexa-aquo in the mutant solution. A comparison of the EXAFS data for wild-type 2-Zn ImiS and the mutant, 2-Zn ImiS (M146I), shows a dramatic effect of the mutation on the average primary coordination sphere of Zn (Figure 5). The first shell features are nearly restored to those of the wild-type enzyme, with a slightly lower amplitude in the high *R* shoulder, previously ascribed to Zn−S scattering. Single-scattering, first shell fits

Table 1: EXAFS Curve Fitting Results for 1-Zn and 2-Zn Forms of ImiS[a]

	model	Zn−N/O	Zn−S	Zn−His[b]	R_f[c]	R_u
			1-Zn ImiS			
1-1	4 N/O	2.07 (5.6)			244	255
1-2	3 N/O + 1 S	2.01 (4.5)	2.28 (2.4)		13	73
1-3	3 N/O + 1 S + 1 His	2.01 (4.5)	2.28 (2.3)	2.92 (12), 3.18 (8.7), 4.07 (12), 4.46 (14)	30	47
			1-Zn ImiS + imipenem			
2-1	4 N/O	2.07 (5.8)			316	317
2-2	3 N/O + 1 S	2.02 (2.9)	2.29 (1.6)		26	79
2-3	3 N/O + 1 S + 1 His	2.02 (3.0)	2.29 (1.4)	2.90 (3.6), 3.09 (3.5), 4.02 (36), 4.44 (10)	31	42
			2-Zn ImiS			
3-1	4 N/O	2.10 (1.3)			90	120
3-2	3 N/O + 1 S	2.04 (3.5)	2.33 (3.9)		14	54
3-3	3 N/O + 1 S + 1 His	2.04 (3.6)	2.33 (3.8)	3.01 (2.9), 3.16 (0.4), 3.96 (7.6), 4.51 (27)	20	46
			2-Zn ImiS (M146I)			
4-1	4 N/O	2.06 (7.0)			185	195
4-2	4 N/O + 0.5 S	2.02 (5.4)	2.29 (1.6)		19	84
4-3	3 N/O + 1 S	2.02 (2.5)	2.29 (9.4)		16	86
4-4	4 N/O + 0.5 S + 0.5 His	2.02 (5.5)	2.28 (3.6)	2.88 (6.4), 3.11 (2.4), 4.16 (10), 4.42 (12)	29	36

[a] Distances (Å) and disorder parameters [in parentheses, σ^2 (10^{-3} Å^2)] shown derive from integer or half-integer coordination number fits to filtered EXAFS data [$k = 1-12.4$ Å^{-1}; single scattering, $R = 0.7-2.45$ Å (fits 1-1, 1-2, 2-1, 2-2, 3-1, 3-2, 4-1, 4-2, and 4-3); multiple scattering, $R = 0.1-4.4$ Å (fits 1-3, 2-3, 3-3, and 4-4)]. [b] Multiple-scattering paths represent the combined paths described in the Experimental Procedures. [c] Goodness of fit (R_f for fits to filtered data and R_u for fits to unfiltered data) defined as $1000(\sum_{i=1}^{N}\{[\mathrm{Re}(\chi i_{calcd})]^2 + [\mathrm{Im}(\chi i_{calcd})]^2\})/(\sum_{i=1}^{N}\{[\mathrm{Re}(\chi i_{obs})]^2 + [\mathrm{Im}(\chi i_{obs})]^2\})$, where N is the number of data points.

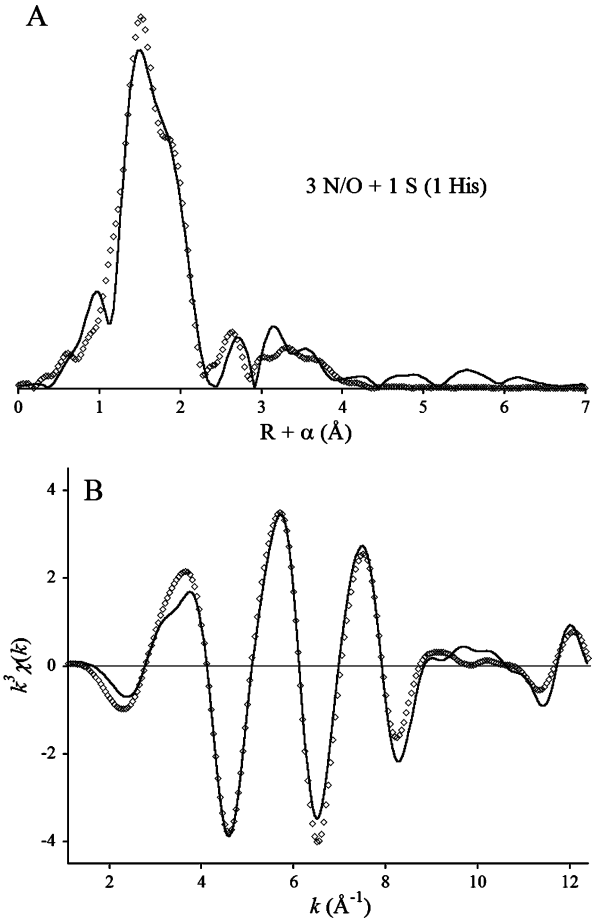

FIGURE 2: Fourier transforms (A) of experimental k^3-weighted EXAFS data (B) for the 1-Zn ImiS imipenem product complex (—) and best multiple-scattering fit (◇).

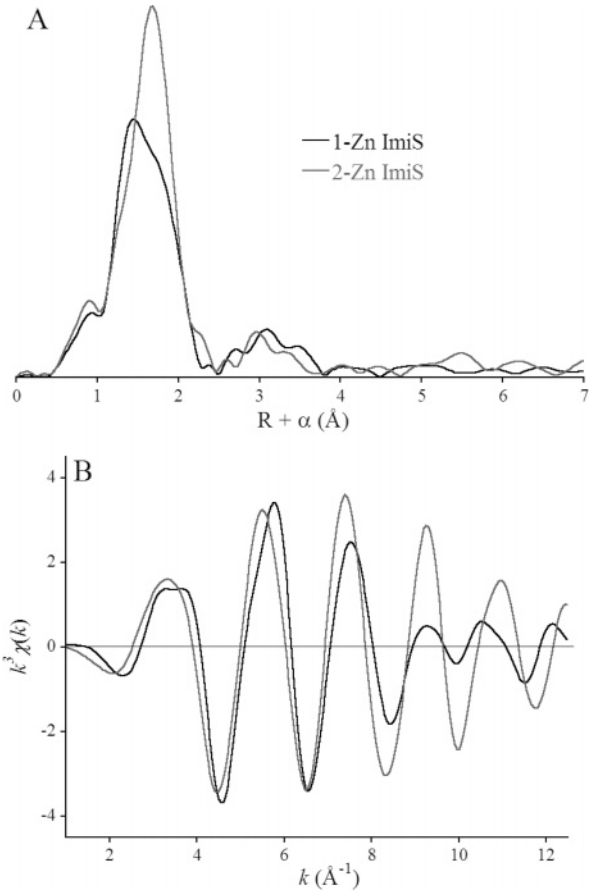

FIGURE 3: Fourier transforms (A) of experimental k^3-weighted EXAFS data (B) for 1-Zn (black line) and 2-Zn (gray line) ImiS.

to the 2-Zn ImiS (M146I) EXAFS, using only low-Z scatterers, shows an average of 4 N/O at 2.06 Å (fit 3-1). Inclusion of one sulfur ligand per Zn ion improves the fit by 92%, although the Debye−Waller factor is a bit large (fit 3-2). Reducing the sulfur contribution to 0.5 S per Zn results in a 90% improvement in the fit residual, with a much more reasonable Debye−Waller factor (fit 3-3). The Zn−S distance in the mutant is restored to that observed for wild-type 1-Zn ImiS, consistent with the loss of the thioether ligand. While the two fits are statistically similar, we favor the model that includes 0.5 S per Zn, owing to the dramatic change that accompanies the mutation and the similarity of

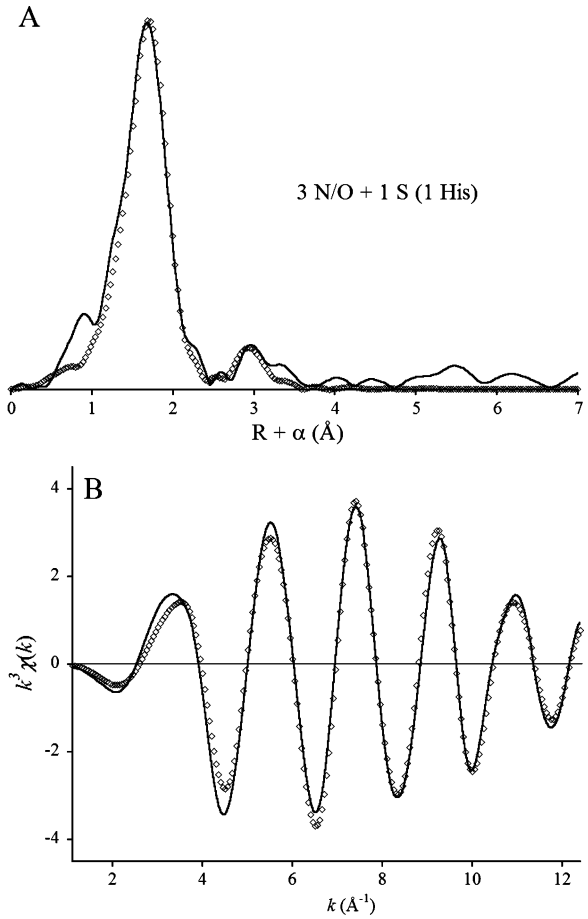

FIGURE 4: Fourier transforms (A) of experimental k^3-weighted EXAFS data (B) for 2-Zn ImiS (—) and best multiple-scattering fit (◇).

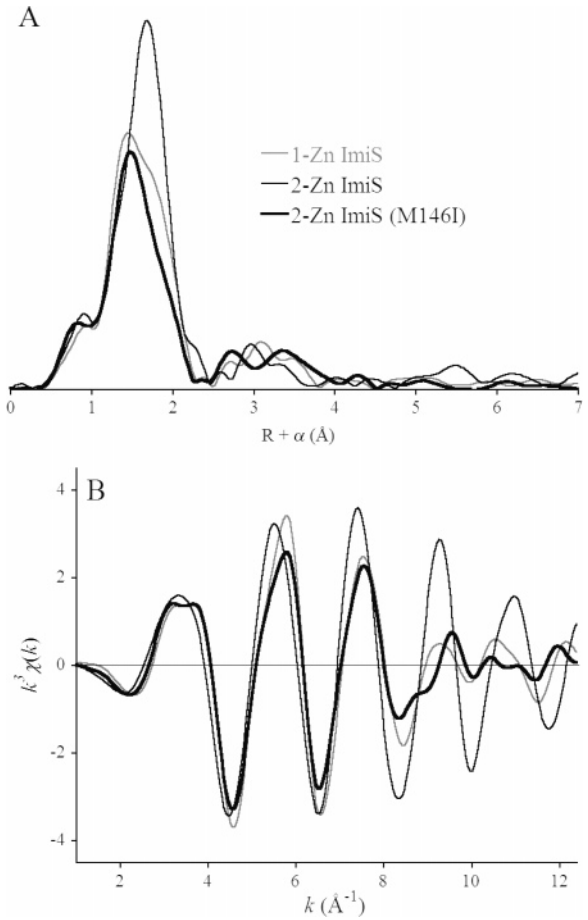

FIGURE 5: Fourier transforms (A) of experimental k^3-weighted EXAFS data (B) for 1-Zn ImiS (gray line), 2-Zn ImiS (thin black line), and 2-Zn ImiS (M146I) mutant (thick black line).

the EXAFS of the mutant to that of the wild-type 1-Zn enzyme. The outer shell scattering is qualitatively affected, although quantitative assessment beyond the presence of 1 ± 0.5 His ligands per Zn ion is difficult. The multiple-scattering fit shown in Figure 6 represents the sum of 4 N/O and 0.5 S in the first shell, with outer shell scattering from 0.5 histidine imidazoles per zinc ion.

DISCUSSION

1-Zn ImiS. Single-scattering fits to the EXAFS data of 1-Zn ImiS show that the first equivalent of zinc is bound to three nitrogen/oxygen donors and one sulfur ligand. This result, in addition to the presence of one coordinated histidine, as indicated by the multiple-scattering fit, supports the conclusion that the first equivalent of Zn^{II} binds at the consensus Zn_2 site. These findings are in agreement with the crystal structure of CphA (*82*), suggesting that this binding mode is general for the class B2 carbapenemases. The EXAFS are also consistent with the metal-binding site determined by UV−vis, EPR, and NMR studies of cobalt-substituted ImiS (*79*), demonstrating that the first equivalent of cobalt occupies the same binding site as the first equivalent of zinc in ImiS.

1-Zn ImiS Plus Imipenem. The EXAFS of the enzyme−product complex of 1-Zn ImiS with imipenem reveals a first shell distance (2.07 Å) that is the same as the resting enzyme, indicating similar coordination numbers in both complexes. The implication of this observation is monodentate binding of the hydrolyzed product. The intensity of the outer shell scattering is also unchanged in the enzyme−product complex FT. This eliminates the possibility of product coordination via the β-lactam nitrogen, which is part of a five-membered ring that remains intact in the hydrolyzed product. The presence of an additional, coordinated rigid ring structure would be expected to give rise to outer shell scattering, similar to that from an additional histidine. While the scattering pattern apparent in Figure 2 is altered relative to the resting enzyme, they exhibit nearly identical amplitudes. An EP complex, which was offered on the basis of stopped-flow kinetics and rapid-freeze quench EPR studies, has recently been hypothesized that is consistent with these data (*86*).

This result is in apparent contrast to the enzyme−product structure determined for CphA with biapenem (*82*), which proposed a hydrolyzed biapenem structure that coordinates zinc in a bidentate fashion, via both the β-lactam nitrogen and the auxiliary carboxylate function. While the EXAFS data presented here cannot distinguish between the carboxylate generated by hydrolysis or the peripheral carboxylate, it clearly does not support bidentate coordination. Given the 98% sequence homology (*85*), it is unlikely that there are significant differences in the substrate-binding pocket. The structures of imipenem and biapenem (Chart 1) are sufficiently similar that they should be expected to produce similar product complexes. The EXAFS data are more consistent with the end-stage product complex, in which the β-lactam nitrogen has been protonated, that was proposed

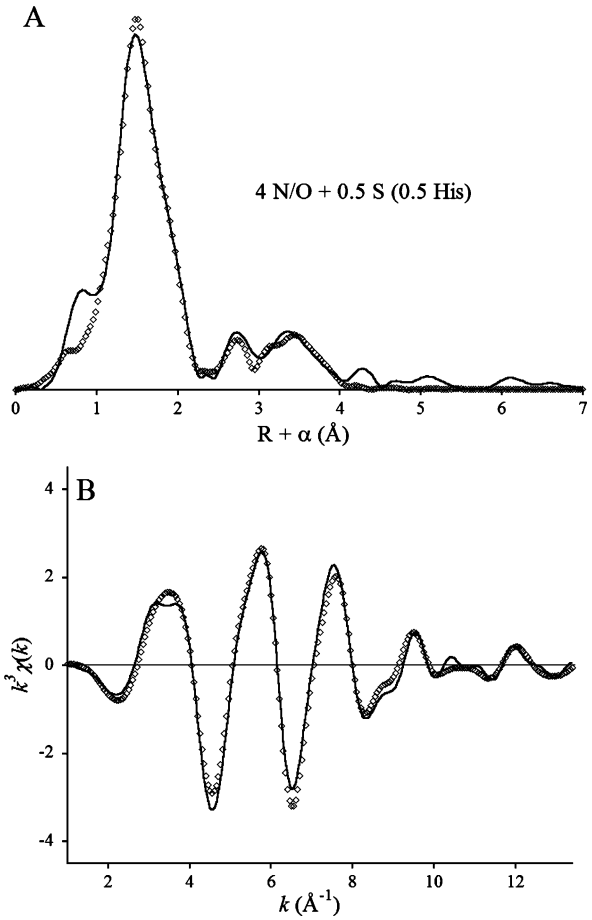

FIGURE 6: Fourier transforms (A) of experimental k^3-weighted EXAFS data (B) for 2-Zn ImiS M146I mutant (—) and best multiple-scattering fit (◇).

Chart 1

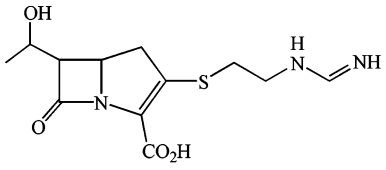

imipenem

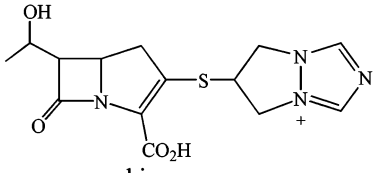

biapenem

by Garau et al. (*82*) but not observed. This may reflect an inability of CphA to transfer a proton to the bound intermediate in the crystal. We see no evidence of inactivation as was seen previously for CphA with moxalactam, where the 3′ leaving group reacted with the active-site cysteinate (*87*).

Inhibitory Zn Site. A comparison of the EXAFS FTs for the active, monozinc and inhibited, dizinc forms of ImiS shows a dramatic change in the average first shell upon binding the inhibitory Zn ion (Figure 3). Single-scattering fits indicate the presence of a coordinated sulfur in the primary coordination sphere of both metal ions. Without a heavy atom coordinated to the inhibitory metal ion, the expected average coordination number is 0.5 S per Zn; increasing the number of S per Zn to 1 improves the fit residual by a factor of 7. Comparing the outer shell scattering of 1-Zn ImiS to 2-Zn ImiS indicates that the average number of histidines per zinc is also approximately the same. The small but measurable increase in the white line intensity for the 2-Zn derivative suggests that the remainder of the coordination sphere of this metal is mostly solvent.

A remote binding site for the second, inhibitory equivalent of metal was previously suggested for the 2-Co analogue of ImiS, on the basis of EPR, NMR, and optical spectroscopy (*79*). The EXAFS data for 2-Zn ImiS are consistent with a remote binding site, on the basis of the lack of an obvious metal−metal interaction and the presence of a sulfur ligand in the coordination sphere of the inhibitory metal ion (Zn binding at the Zn_1 site would be expected to display tetracoordination, including three histidine ligands). The amino acid sequence of ImiS requires that the sulfur ligand in the inhibitory site must come from methionine, because only one Cys is present and it is coordinated to the hydrolytic metal ion.

The four methionines present (M43, M72, M146, and M252) were considered in the context of the crystal structures of CphA with and without biapenem (*82*). Each was examined for location relative to the active site, their effect (if any) on substrate binding, and their distance to nearby histidines residues. M252 was immediately discounted because of its distance from the active site and from the nearest histidine residue (>20 Å). M43 and M72 are both conserved in class B1 and B3 MβLs, which maintain activity upon binding a second zinc(II) ion. Therefore, their involvement in zinc inhibition was considered unlikely. M43 is ∼14 Å from the active site and is within 10 Å of H96, but neither M43 nor H96 participate in substrate binding or the proposed hydrolytic mechanism (*80*, *82*). M72 is ca. 13 Å from both the zinc ion and H263, which coordinates the active Zn ion and helps stabilize the intermediate (*80*−*82*). However, M72 is most likely too distant from H263 for a second zinc(II) ion to bind both H263 and M72. We see no evidence that H263 dissociates from the first Zn ion (this is the only histidine coordinated by the hydrolytic metal ion). Therefore, both M43 and M72 were dismissed as potential ligands of the inhibitory zinc ion.

The remaining methionine, M146, is located on the elongated α3 helix (formed by residues R140−L161) that is unique to class B2 MβLs. In contrast to reported B1 and B3 structures (*16*, *19*, *20*, *22*, *28*), this extended helix is located near the active-site groove and contains hydrophobic residues that appear to help define the active site (*82*). M146 is near the beginning of this helix, directly behind H118, which has been proposed to activate the hydrolytic water molecule through a hydrogen-bonding interaction.

Mutation of M146 to isoleucine *abolishes* inhibition by a second equivalent of Zn and has a profound effect on the EXAFS, as shown in Figure 5 and Table 1. Given the specificity with which wild-type ImiS binds the second Zn, it seems unlikely that it is nonspecifically bound in the mutant. The XANES of the mutant shows a dramatic increase in white line absorption, suggesting that the second equivalent of Zn coordinates multiple water ligands (Figure S1 in the Supporting Information). The EXAFS of the 2-Zn M146I mutant clearly indicates a loss of a sulfur ligand. We propose that the inhibitory zinc ion binds to both M146 and H118 in

Scheme 1

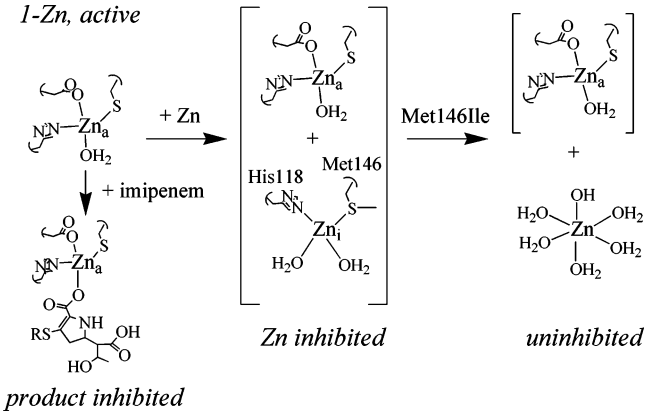

wild-type ImiS. The consequences of this binding mode are 2-fold. In addition to bridging the active-site loop (M146) and the substrate-binding groove (H118), this mode of coordination could also turn H118 away from the active site, making it unavailable for activation of the hydrolytic water molecule, further inhibiting catalysis. The location of this inhibitory site is not conserved in class B1 and B3 lactamases, explaining the lack of similar behavior in these enzymes.

SUMMARY

Results of these studies are summarized graphically in Scheme 1. The EXAFS data presented here provide the first spectroscopic interrogation of ImiS from *A. veronii bv. sobria* with its native metal, zinc, in both the hydrolytically active, monozinc form (with and without bound product) and the inhibited, dizinc form. The results for 1-Zn ImiS confirm the first equivalent of zinc binds to the Zn_2 site, consistent with previous spectroscopic characterization of the Co^{II}-substituted enzyme (*79*) and the crystal structure of CphA (*82*). EXAFS of the product-bound form of 1-Zn ImiS with imipenem indicates that the product is bound in a monodentate fashion, through a carboxylate ligand, suggesting that the product-bound species isolated here is the end-stage product complex implied but not observed in X-ray diffraction studies of CphA (*82*). EXAFS of 2-Zn ImiS (wild type) and 2-Zn ImiS (M146I) support three conclusions: (1) the second equivalent of zinc binds to a location remote from the active site; (2) the ligand set of the inhibitory metal ion includes the sulfur of M146; and (3) a histidine, most likely H118, is also coordinated by the inhibitory metal ion. These data provide the first structural information regarding the inhibitory binding site and offer some explanation for the lack of this behavior in class B1 and B3 lactamases.

SUPPORTING INFORMATION AVAILABLE

Figure S1, comparing the XANES of 1-Zn ImiS, 1-Zn ImiS plus imipenem, 2-Zn ImiS, and 2-Zn ImiS (M146I). This material is available free of charge via the Internet at http://pubs.acs.org.

REFERENCES

1. Bush, K., Jacoby, G. A., and Medeiros, A. A. (1995) A Functional Classification Scheme for β-Lactamases and Its Correlation with Molecular Structure, *Antimicrob. Agents Chemother. 39*, 1211−1233.
2. Knowles, J. R. (1985) Penicillin Resistance: The Chemistry of β-Lactamase Inhibition, *Acc. Chem. Res. 18*, 97−104.
3. Cricco, J. A., Orellano, E. G., Rasia, R. M., Ceccarelli, E. A., and Vila, A. J. (1999) Metallo-β-lactamases: Does It Take Two to Tango? *Coord. Chem. Rev. 190*−*192*, 519−535.
4. Crowder, M. W., and Walsh, T. R. (1999) Metallo-β-lactamases: Structure and Function, *Research Signpost 3*, 105−132.
5. Wang, Z., Fast, W., Valentine, A. M., and Benkovic, S. J. (1999) Metallo-β-lactamases: Structure and Mechanism, *Curr. Opin. Chem. Biol. 3*, 614−622.
6. Bush, K. (1998) Metallo-β-lactamases: A Class Apart, *Clin. Infect. Dis. 27*, S48−S53.
7. Davies, R. B., and Abraham, E. P. (1974) Metal Cofactor Requirements of β-Lactamase II, *Biochem. J. 143*, 129−135.
8. Ambler, R. P., Daniel, M., Fleming, J., Hermoso, J., Pang, C., and Waley, S. G. (1985) The Amino Acid Sequence of the Zinc-Requiring β-Lactamase II from the Bacterium *Bacillus cereus* 569, *FEBS Lett. 189*, 207−211.
9. Crowder, M. W., Wang, Z., Franklin, S. L., Zovinka, E. P., and Benkovic, S. J. (1996) Characterization of the Metal-Binding Sites of the β-Lactamase from *Bacteroides fragilis*, *Biochemistry 35*, 12126−12132.
10. Wang, Z., and Benkovic, S. J. (1998) Purification, Characterization, and Kinetic Studies of a Soluble *Bacteroides fragilis* Metallo-β-lactamase That Provides Multiple Antibiotic Resistance, *J. Biol. Chem. 2736*, 22402−22408.
11. Crowder, M. W., Walsh, T. R., Banovic, L., Pettit, M., and Spencer, J. (1998) Overexpression, Purification, and Characterization of the Cloned Metallo-β-lactamase L1 from *Stenotrophomonas maltophilia*, *Antimicrob. Agents Chemother. 42*, 921−926.
12. Bellais, S., Aubert, D., Naas, T., and Nordmann, P. (2000) Molecular and Biochemical Heterogeneity of Class B Carbapenem-Hydrolyzing β-Lactamases in *Chryseobacterium meningosepticum*, *Antimicrob. Agents Chemother. 44*, 1878−1886.
13. Rasmussen, B. A., and Bush, K. (1997) Carbapenem-Hydrolyzing β-Lactamases, *Antimicrob. Agents Chemother. 41*, 223−232.
14. Rossolini, G. M., Franceschini, N., Riccio, M. L., Mercuri, P. S., Perilli, S., Galleni, M., Frere, J. M., and Amicosante, G. (1998) Characterization and Sequence of the *Chryseobacterium (Flavobacterium) meningosepticum* Carbapenemase: A New Molecular Class B β-Lactamase Showing a Broad Substrate Profile, *Biochem. J. 332*, 145−152.
15. Carfi, A., Pares, S., Duee, E., Galleni, M., Duez, C., Frere, J. M., and Dideberg, O. (1995) The 3-D Structure of a Zinc Metallo-β-lactamase from *Bacillus cereus* Reveals a New Type of Protein Fold, *EMBO J. 14*, 4914−4921.
16. Concha, N. O., Rasmussen, B. A., Bush, K., and Herzberg, O. (1996) Crystal Structure of the Wide-Spectrum Binuclear Zinc β-Lactamase from *Bacteroides fragilis*, *Structure 4*, 823−836.
17. Fitzgerald, P. M. D., Wu, J. K., and Toney, J. H. (1998) Unanticipated Inhibition of the Metallo-β-lactamase from *Bacteroides fragilis* by 4-Morpholineethanesulfonic Acid (MES): A Crystallographic Study at 1.85 Å Resolution, *Biochemistry 37*, 6791−6800.
18. Carfi, A., Duee, E., Galleni, M., Frere, J.-M., and Dideberg, O. (1998) 1.85 Å Resolution Structure of the Zinc(II) β-Lactamase from *Bacillus cereus*, *Acta Crystallogr., Sect. D: Biol. Crystallogr. 54*, 313−323.
19. Fabiane, S. M., Sohi, M. K., Wan, T., Payne, D. J., Bateson, J. H., Mitchell, T., and Sutton, B. J. (1998) Crystal Structure of the Zinc-Dependent β-Lactamase from *Bacillus cereus* at 1.9 Å Resolution: Binuclear Active Site with Features of a Mononuclear Enzyme, *Biochemistry 37*, 12404−12411.
20. Ullah, J. H., Walsh, T. R., Taylor, I. A., Emery, D. C., Verma, C. S., Gamblin, S. J., and Spenser, J. (1998) The Crystal Structure of the L1 Metallo-β-lactamase from *Stenotrophomonas maltophila* at 1.7 Å Resolultion, *J. Mol. Biol. 287*, 125−136.
21. Li, Z., Rasmussen, B. A., and Herzberg, O. (1999) Structural Consequences of the Active Site Substitution Cys181-Ser in Metallo-β-lactamase from *Bacteroides fragilis*, *Protein Sci. 8*, 249−252.
22. Concha, N. O., Janson, C. A., Rowling, P., Pearson, S., Cheever, C. A., Clarke, B. P., Lewis, C., Galleni, M., Frere, J. M., Payne, D. J., Bateson, J. H., and Abdel-Meguid, S. S. (2000) Crystal Structure of the IMP-1 Metallo-β-lactamase from *Pseudomonas aeruginosa* and Its Complex with a Mercaptocarboxylate Inhibitor: Binding Determinants of a Potent, Broad-Spectrum Inhibitor, *Biochemistry 39*, 4288−4298.
23. Toney, J. H., Hammond, G. G., Fitzgerald, P. M. D., Sharma, N., Balkovec, J. M., Rouen, G. P., Olson, S. H., Hammond, M. L.,

Greenlee, M. L., and Gao, Y.-D. (2001) Succinic Acids as Potent Inhibitors of Plasmid-Borne IMP-1 Metallo-β-lactamase, *J. Biol. Chem. 276*, 31913−31918.

24. Garcia-Saez, I., Mercuri, P. S., Papamicael, C., Kahn, R., Frere, J.-M., Galleni, M., Rossolini, G. M., and Dideberg, O. (2003) Three-Dimensional Structure of FEZ-1, a Monomeric Subclass B3 Metallo-β-lactamase from *Fluoribacter gormanii*, in Native Form and in Complex with D-Captopril, *J. Mol. Biol. 325*, 651−660.
25. Garcia-Saez, I., Hopkins, J., Papamicael, C., Franceschini, N., Amicosante, G., Rossolini, G. M., Galleni, M., Frere, J.-M., and Dideberg, O. (2003) The 1.5 Å Structure of *Chryseobacterium meningosepticum* Zinc β-Lactamase in Complex with the Inhibitor, D-Captopril, *J. Biol. Chem. 278*, 23868−23873.
26. Davies, A. M., Rasia, R. M., Vila, A. J., Sutton, B. J., and Fabiane, S. M. (2005) Effect of pH on the Active Site of an Arg121Cys Mutant of the Metallo-β-lactamase from *Bacillus cereus*: Implications for the Enzyme Mechanism, *Biochemistry 44*, 4841−4849.
27. Yamaguchi, Y., Kuroki, T., Yasuzawa, H., Higashi, T., Jin, W., Kawanami, A., Yamagata, Y., Arakawa, Y., Goto, M., and Kurosaki, H. (2005) Probing the Role of Asp-120(81) of Metallo-β-lactamase (IMP-1) by Site-Directed Mutagenesis, Kinetic Studies, and X-ray Crystallography, *J. Biol. Chem. 280*, 20824−20832.
28. Spencer, J., Read, J., Sessions, R. B., Howell, S., Blackburn, G. M., and Gamblin, S. J. (2005) Antibiotic Recognition by Binuclear Metallo-β-lactamases Revealed by X-ray Crystallography, *J. Am. Chem. Soc. 127*, 14439−14444.
29. Murphy, T. A., Catto, L. E., Halford, S. E., Hadfield, A. T., Minor, W., and Spencer, T. R. (2006) Crystal Structure of *Pseudomonas aeruginosa* SPM-1 Provides Insights into Variable Zinc Affinity of Metallo-β-lactamases, *J. Mol. Biol. 357*, 890−903.
30. Baldwin, G. S., Galdes, A., Hill, H. A. O., Smith, B. E., Waley, S. G., and Abraham, E. P. (1978) Histidine Residues as Zinc Ligands in β-Lactamase II, *Biochem. J. 175*, 441−447.
31. Galdes, A., Hill, H. A. O., Baldwin, G. S., Waley, S. G., and Abraham, E. P. (1980) The Proton Nuclear Magnetic Resonance Spectroscopy of Cobalt(II)-β-Lactamase II, *Biochem. J. 187*, 789−795.
32. Baldwin, G. S., Galdes, A., Hill, H. A. O., Waley, S. G., and Abraham, E. P. (1980) A Spectroscopic Study of Metal Ion and Ligand Binding to β-Lactamase II, *J. Inorg. Biochem. 13*, 189−204.
33. Bicknell, R., Schaffer, A., Waley, S. G., and Auld, D. S. (1986) Changes in the Coordination Geometry of the Active Site Metal during Catalysis of Benzylpenicillin Hydrolysis by *Bacillus cereus* β-Lactamase II, *Biochemistry 25*, 7208−7215.
34. Orellano, E. G., Giardini, J. E., Cricco, J. A., and Vila, A. J. (1998) Spectroscopic Characterization of a Binuclear Metal Site in *Bacillus cereus* β-Lactamase II, *Biochemistry 37*, 10173−10180.
35. Scrofani, S. D. B., Chung, J., Huntley, J. J. A., Benkovic, S. J., Wright, P. E., and Dyson, H. J. (1999) NMR Characterization of the Metallo-β-lactamase from *Bacteroides fragilis* and Its Interaction with a Tight-Binding Inhibitor: Role of an Active-Site Loop, *Biochemistry 38*, 14507−14514.
36. deSeny, D., Heinz, U., Wommer, S., Kiefer, M., Meyer-Klaucke, W., Galleni, M., Frere, J. M., Bauer, R., and Adolph, H. W. (2001) Metal Ion Binding and Coordination Geometry for Wild Type and Mutants of Metallo-β-lactamase from *Bacillus cereus* 569/H/9 (BcII), *J. Biol. Chem. 276*, 45065−45078.
37. Estiu, G. L., Rasia, R. M., Cricco, J. A., Vila, A. J., and Zerner, M. C. (2002) Is There a Bridging Ligand in Metal-Substituted Zinc β-Lactamases? A Spectroscopic and Theoretical Answer, *Int. J. Quantum Chem. 88*, 118−132.
38. Garrity, J. D., Pauff, J. M., and Crowder, M. W. (2004) Probing the Dynamics of a Mobile Loop Above the Active Site of L1, a Metallo-β-lactamase from *Stenotrophomonas maltophilia*, via Site-Directed Mutagenesis and Stopped-Flow Fluorescence Spectroscopy, *J. Biol. Chem. 279*, 39663−39670.
39. Garrity, J. D., Bennett, B., and Crowder, M. W. (2005) Direct Evidence that the Reaction Intermediate of Metallo-β-lactamase L1 is Metal Bound, *Biochemistry 44*, 1078−1087.
40. Schilling, O., Vogel, A., Kostelecky, B., daLuz, H. N., Spemann, D., Spaeth, B., Marchfelder, A., Troeger, W., and Meyer-Klaucke, W. (2005) Zinc- and Iron-Dependent Cytosolic Metallo-β-lactamase Domain Proteins Exhibit Similar Zinc-Binding Affinities, Independent of an Atypical Glutamate at the Metal-Binding Site, *Biochem. J. 385*, 145−153.
41. Periyannan, G., Costello, A. L., Tierney, D. L., Yang, K.-W., Bennett, B., and Crowder, M. W. (2006) Sequential Binding of Cobalt(II) to Metallo-β-lactamase CcrA, *Biochemistry 45*, 1313−1320.
42. Costello, A. L., Periyannan, G., Yang, K.-W., Crowder, M. W., and Tierney, D. L. (2006) Site Selective Binding of Zn(II) to Metallo-β-lactamase L1 from *Stenotrophomonas maltophilia*, *J. Biol. Inorg. Chem. 11*, 351−358.
43. Payne, D. J., Bateson, J. H., Gasson, B. C., Proctor, D., Khushi, T., Farmer, T. H., Tolson, D. A., Bell, D., Skett, P. W., Marshall, A. C., Reid, R., Ghosez, L., Combret, Y., and Marchand-Brynaert, J. (1997) Inhibition of Metallo-β-lactamases by a Series of Mercaptoacetic Acid Thiol Ester Derivatives, *Antimicrob. Agents Chemother. 41*, 135−140.
44. Wang, Z., Fast, W., and Benkovic, S. J. (1998) Direct Observation of an Enzyme-Bound Intermediate in the Catalytic Cycle of the Metallo-β-lactamase from *Bacteroides fragilis*, *J. Am. Chem. Soc. 120*, 10788−10789.
45. Bounaga, S., Laws, A. P., Galleni, M., and Page, M. I. (1998) The Mechanism of Catalysis and the Inhibition of the *Bacillus cereus* Zinc-Dependent β-Lactamase, *Biochem. J. 331*, 703−711.
46. Yang, Y., Keeney, D., Tang, X., Canfield, N., and Rasmussen, B. A. (1999) Kinetic Properties and Metal Content of the Metallo-β-lactamse CcrA Harboring Selective Amino Acid Substitutions, *J. Biol. Chem. 274*, 15706−15711.
47. McManus-Munoz, S., and Crowder, M. W. (1999) Kinetic Mechanism of Metallo-β-lactamase L1 from *Stenotrophomonas maltophilia*, *Biochemistry 38*, 1547−1553.
48. Wang, Z., Fast, W., and Benkovic, S. J. (1999) On the Mechanism of the Metallo-β-lactamase from *Bacteroides fragilis*, *Biochemistry 38*, 10013−10023.
49. Paul-Soto, R., Bauer, R., Frere, J. M., Galleni, M., Meyer-Klaucke, W., Nolting, H., Rossolini, G. M., deSeny, D., Hernandez-Vallardes, M., Zeppezauer, M., and Adolph, H. W. (1999) Mono- and Binuclear Zn^{2+}-β-lactamase: Role of the Conserved Cysteine in the Catalytic Mechanism, *J. Biol. Chem. 274*, 13242−13249.
50. Chantalat, L., Duee, E., Galleni, M., Frere, J.-M., and Dideberg, O. (2000) Structural Effects of the Active Site Mutation Cysteine to Serine in *Bacillus cereus* Zinc-β-lactamase, *Protein Sci. 9*, 1402−1406.
51. Franceschini, N., Caravelli, B., Docquier, J.-D., Galleni, M., Frere, J.-M., Amicosante, G., and Rossolini, G. M. (2000) Purification and Biochemical Characterization of the VIM-1 Metallo-β-lactamase, *Antimicrob. Agents Chemother. 44*, 3003−3007.
52. Yanchak, M. P., Taylor, R. A., and Crowder, M. W. (2000) Mutational Analysis of Metallo-β-lactamase CcrA from *Bacteroides fragilis*, *Biochemistry 39*, 11330−11339.
53. Fast, W., Wang, Z., and Benkovic, S. J. (2001) Familial Mutations and Zinc Stoichiometry Determine the Rate-Limiting Step of Nitrocefin Hydrolysis by Metallo-β-lactamase from *Bacteroides fragilis*, *Biochemistry 40*, 1640−1650.
54. Simm, A. M., Higgins, C. S., Carenbauer, A. L., Crowder, M. W., Bateson, J. H., Bennett, P. M., Clarke, A. R., Halford, S. E., and Walsh, T. R. (2002) Characterization of Monomeric L1 Metallo-β-lactamase and the Role of the N-Terminal Extension in Negative Cooperativity and Antibiotic Hydrolysis, *J. Biol. Chem. 277*, 24744−24751.
55. Prosperi-Meys, C., DeSeny, D., Llabres, G., Galleni, M., and Lamotte-Brasseur, J. (2002) Active-Site Mutants of Class B β-lactamases: Substrate Binding and Mechanistic Study, *Cell. Mol. Life Sci. 59*, 2136−2143.
56. Murphy, T. A., Simm, A. M., Toleman, M. A., Jones, R. N., and Walsh, T. W. (2003) Biochemical Characterization of the Acquired Metallo-β-lactamase SPM-1 from *Pseudomonas aeruginosa*, *Antimicrob. Agents Chemother. 47*, 582−587.
57. Periyannan, G., Shaw, P. J., Sigdel, T., and Crowder, M. W. (2004) In Vivo Folding of Recombinant Metallo-β-lactamase L1 Requires the Presence of Zn(II), *Protein Sci. 13*, 2236−2243.
58. Mercuri, P. S., Garcia-Saez, I., DeVriendt, K., Thamm, I., Devreese, B., VanBeeumen, J., Dideberg, O., Rossolini, G. M., Frere, J.-M., and Galleni, M. (2004) Probing the Specificity of the Subclass B3 FEZ-1 Metallo-β-lactamase by Site-Directed Mutagenesis, *J. Biol. Chem. 279*, 33630−33638.
59. Olsen, L., Jost, S., Adolph, H.-W., Pettersson, I., Hemmingsen, L., and Jorgensen, F. S. (2006) New Leads of Metallo-β-lactamase Inhibitors from Structure-Based Pharmacophore Design, *Bioorg. Med. Chem. 14*, 2627−2635.

60. Gilson, H. S. R., and Krauss, M. (1999) Structure and Spectroscopy of Metallo-lactamase Active Sites, *J. Am. Chem. Soc. 121*, 6984−6989.
61. Diaz, N., Suarez, D., and Merz, K. M., Jr. (2000) Zinc Metallo-β-lactamase from *Bacteroides fragilis*: A Quantum Chemical Study on Model Systems of the Active Site, *J. Am. Chem. Soc. 122*, 4197−4208.
62. Diaz, N., Suarez, D., and Merz, K. M., Jr. (2001) Molecular Dynamics Simulations of the Mononuclear Zinc β-Lactamase from *Bacillus cereus* Complexed with Benzylpenicillin and a Quantum Chemical Study of the Reaction Mechanism, *J. Am. Chem. Soc. 123*, 9867−9879.
63. Krauss, M., Gilson, H. S. R., and Gresh, N. (2001) Structure of the First-Shell Active Site in Metallolactamase: Effect of Water Ligands, *J. Phys. Chem. B 105*, 8040−8049.
64. Prosperi-Meys, C., Wouters, J., Galleni, M., and Lamotte-Brasseur, J. (2001) Substrate Binding and Catalytic Mechanism of Class B β-Lactamases: A Molecular Modelling Study, *Cell. Mol. Life Sci. 58*, 2136−2143.
65. Gu, W., Zhu, J., and Liu, H. (2002) Different Protonation States of the *Bacillus cereus* Binuclear Zinc Metallo-β-lactamase Active Site Studied by Combined Quantum Mechanical and Molecular Mechanical Simulations, *J. Theor. Comp. Chem. 1*, 69−80.
66. Olsen, L., Antony, J., Hemmingsen, L., and Mikkelsen, K. V. (2002) Structure of a Metal Ion Binding Site in β-Lactamase: Quantum Mechanical Study of the Influence of Hydrogen-Bonding Network and Backbone Constraints, *J. Phys. Chem. A 106*, 1046−1053.
67. Oelschlaeger, P., Schmid, R. D., and Pleiss, J. (2003) Insight into the Mechanism of the IMP-1 Metallo-β-lactamase by Molecular Dynamics Simulations, *Protein Eng. 16*, 341−350.
68. Krauss, M., Gresh, N., and Antony, J. (2003) Binding and Hydrolysis of Ampicillin in the Active Site of a Zinc Lactamase, *J. Phys. Chem. B 107*, 1215−1229.
69. Dal Peraro, M., Vila, A. J., and Carloni, P. (2004) Substrate Binding to Mononuclear Metallo-β-lactamase from *Bacillus cereus*, *Proteins: Struct., Funct., Bioinf. 54*, 412−423.
70. Antony, J., Piquemal, J.-P., and Gresh, N. (2005) Complexes of Thiomandelate and Captopril Mercaptocarboxylate Inhibitors to Metallo-β-lactamase by Polarizable Molecular Mechanics. Validation on Model Binding Sites by Quantum Chemistry, *J. Comput. Chem. 26*, 1131−1147.
71. Park, H., Brothers, E. N., and Merz, K. M., Jr. (2005) Hybrid QM/MM and DFT Investigations of the Catalytic Mechanism and Inhibition of the Dinuclear Zinc Metallo-β-lactamase CcrA from *Bacteroides fragilis*, *J. Am. Chem. Soc. 127*, 4232−4241.
72. Lopez, R., Menendez, M. I., Diaz, N., Suarez, D., Campomanes, P., Ardura, D., and Sordo, T. L. (2006) Theoretical Studies on the Ring Opening of β-Lactams: Processes in Solution and in Enzymatic Media, *Curr. Org. Chem. 10*, 805−821.
73. Segatore, B., Massida, O., Satta, G., Setacci, D., and Amicosante, G. (1993) High Specificity of CphA-Encoded Metallo-β-lactamase from *Aeromonas hydrophila* AE036 for Carbapenems and Its Contribution to β-Lactam Resistance, *Antimicrob. Agents Chemother. 37*, 1324−1328.
74. Felici, A., and Amicosante, G. (1995) Kinetic Analysis of Extension of Substrate Specificity with *Xanthomonas maltophila*, *Aeromonas hydrophila*, and *Bacillus cereus* Metallo-β-lactamases, *Antimicrob. Agents Chemother. 39*, 192−199.
75. Walsh, T. R., Gamblin, S., Emery, D. C., MacGowan, A. P., and Bennett, P. M. (1996) Enzyme Kinetics and Biochemical Analysis of ImiS, the Metallo-β-lactamase from *Aeromonas sobria* 163a, *J. Antimicrob. Chemother. 37*, 423−431.
76. Vallardes, M. H., Feilici, A., Weber, G., Adolph, H. W., Zeppezauer, M., Rossolini, G. M., Amicosante, G., Frere, J. M., and Galleni, M. (1997) Zn(II) Dependence of the *Aeromonas hydrophila* AE036 Metallo-β-Lactamase Activity and Stability, *Biochemistry 36*, 11534−11541.
77. Vallardes, M. H., Kiefer, M., Heinz, U., Soto, R. P., Meyer-Klaucke, W., Nolting, H. F., Zeppezauer, M., Galleni, M., Frere, J. M., and Rossolini, G. M. (2000) Kinetic and Spectroscopic Characterization of Native and Metal-Substituted β-Lactamase from *Aeromonas hydrophila* AE036, *FEBS Lett. 467*, 221−225.
78. Crawford, P. A., Sharma, N., Chandrasekar, S., Sigdel, T., Walsh, T. R., Spencer, J., and Crowder, M. W. (2004) Over-expression, Purification and Characterization of Metallo-β-Lactamase imiS from *Aeromonas veronii bv. sobria*, *Protein Expression Purif. 36*, 272−279.
79. Crawford, P. A., Yang, K. W., Sharma, N., Bennett, B., and Crowder, M. W. (2005) Spectroscopic Studies on Cobalt(II)-Substituted Metallo-β-lactamase ImiS from *Aeromonas veronii bv. sobria*, *Biochemistry 44*, 5168−5176.
80. Xu, D., Zhou, Y., Xie, D., and Guo, H. (2005) Antibitoic Binding to Monozinc CphA β-Lactamase from *Aeromonas hydrophila*: Quantum Mechanical/Molecular Mechanical and Density Functional Theory Studies, *J. Med. Chem. 48*, 6679−6689.
81. Xu, D., Xie, D., and Guo, H. (2006) Catalytic Mechanism of Class B2 Metallo-β-lactamase, *J. Biol. Chem. 281*, 8740−8747.
82. Garau, G., Bebrone, C., Anne, C., Galleni, M., Frere, J., and Dideberg, O. (2005) A Metallo-β-lactamase Enzyme in Action: Crystal Structures of the Monozinc Carbapenemase CphA and Its Complex with Biapenem, *J. Mol. Biol. 345*, 785−795.
83. Thomas, P. W., Stone, E. M., Costello, A. L., Tierney, D. L., and Fast, W. (2005) The Quorum-Quenching Lactonase from *Bacillus thuringiensis* Is a Metalloprotein, *Biochemistry 44*, 7559−7565.
84. McClure, C. P., Rusche, K. M., Peariso, K., Jackman, J. E., Fierke, C. A., and Penner-Hahn, J. E. (2003) EXAFS Studies of the Zinc Sites of UDP-(3-*O*-acyl)-*N*-acetylglucosamine Deacetylase (LpxC), *J. Inorg. Biochem. 94*, 78−85.
85. Walsh, T. R., Neville, W. A., Haran, M. H., Tolson, D., Payne, D. J., Bateson, J. H., MacGowan, A. P., and Bennett, P. M. (1998) Nucleotide and Amino Acid Sequences of the Metallo-β-lactamase, ImiS, from *Aeromonas veronii bv. sobria*, *Antimicrob. Agents Chemother. 42*, 436−439.
86. Sharma, N. P., Hajdin, C., Chandrasekar, S., Bennett, B., Yang, K.-W., and Crowder, M. W. (2006) Mechanistic Studies on the Mononuclear Zn(II)-Containing Metallo-β-lactamase ImiS from *Aeromonas sobria*, *Biochemistry*, in press.
87. Zersoven, A., Vallardes, M. H., Devreese, B., Prosperi-Meys, C., Adolph, H.-W., Mercuri, P. S., Vanhove, M., Amicosante, G., van Beeumen, J., Frere, J.-M., and Galleni, M. (2001) Inactivation of *Aeromonas hydrophila* Metallo-β-lactamase by Cephamycins and Moxalactam, *Eur. J. Biochem. 268*, 3840−3850.

BI061547E